ELSEVIER

NeuroImage

www.elsevier.com/locate/ynimg
NeuroImage 37 (2007) S59–S70

Computer simulation of glioma growth and morphology

Hermann B. Frieboes,[a,b] John S. Lowengrub,[b,e,1] S. Wise,[b] X. Zheng,[b] Paul Macklin,[b] Elaine L. Bearer,[c,d,2] and Vittorio Cristini[a,*,3]

[a]*School of Health Information Sciences, The University of Texas Health Science Center at Houston, USA*
[b]*Department of Mathematics, University of California, Irvine, USA*
[c]*Department of Pathology and Laboratory Medicine, Brown University Medical School, USA*
[d]*California Institute of Technology, USA*
[e]*Department of Biomedical Engineering, University of California, Irvine, USA*

Received 1 February 2007; revised 1 March 2007; accepted 2 March 2007
Available online 23 March 2007

Despite major advances in the study of glioma, the quantitative links between intra-tumor molecular/cellular properties, clinically observable properties such as morphology, and critical tumor behaviors such as growth and invasiveness remain unclear, hampering more effective coupling of tumor physical characteristics with implications for prognosis and therapy. Although molecular biology, histopathology, and radiological imaging are employed in this endeavor, studies are severely challenged by the multitude of different physical scales involved in tumor growth, i.e., from molecular nanoscale to cell microscale and finally to tissue centimeter scale. Consequently, it is often difficult to determine the underlying dynamics across dimensions. New techniques are needed to tackle these issues. Here, we address this multi-scalar problem by employing a novel *predictive* three-dimensional mathematical and computational model based on first-principle equations (conservation laws of physics) that describe mathematically the diffusion of cell substrates and other processes determining tumor mass growth and invasion. The model uses conserved variables to represent known determinants of glioma behavior, e.g., cell density and oxygen concentration, as well as biological functional relationships and parameters linking phenomena at different scales whose specific forms and values are hypothesized and calculated based on in vitro and in vivo experiments and from histopathology of tissue specimens from human gliomas. This model enables correlation of glioma morphology to tumor growth by quantifying interdependence of tumor mass on the microenvironment (e.g., hypoxia, tissue disruption) and on the cellular phenotypes (e.g., mitosis and apoptosis rates, cell adhesion strength). Once functional relationships between variables and associated parameter values have been informed, e.g., from histopathology or intra-operative analysis, this model can be used for disease diagnosis/prognosis, hypothesis testing, and to guide surgery and therapy. In particular, this tool identifies and quantifies the effects of vascularization and other cell-scale glioma morphological characteristics as predictors of tumor-scale growth and invasion.

Keywords: Glioma; Glioblastoma; Computer simulation; 3D; Tumor growth; Tumor morphology; Mathematical model; Cancer model

Introduction

Generic molecular mechanisms and cell-scale migration dynamics are well described (Friedl and Wolf, 2003; Keller et al., 2006; Sierra, 2005; Van Kempen et al., 2003; Wolf and Friedl, 2006; Kopfstein and Christofori, 2006; Yamaguchi et al., 2005; Elvin and Garner, 2005; Sahai, 2005; Friedl et al., 2004; Friedl, 2004; Condeelis et al., 2005; Ridley et al., 2003) to the point that therapies designed with this knowledge have been recently employed to attempt to curtail or prevent growth and invasion of various cancers. However, the effects of therapies are often inadequate or their benefits unclear. 3D culture and in vivo studies of effects of cell adhesion molecules (CAM) and matrix metalloproteinases (MMP) on cell migration have yielded inconsistent results (Friedl and Wolf, 2003; Toker and Yoeli-Lerner, 2006; Khoshyomn et al., 1999; Giese et al., 1996), and data on the function of proteases in tumor invasion and metastasis are not completely as expected (Friedl and Wolf, 2003). Pharmacological inhibitors that regulate cell adhesion are being employed in anti-invasive therapy to treat various cancers (McLean et al., 2005; Yin et al., 2006; Lockett et al., 2006; Lah et al., 2006; Eble and Haier, 2006; Hayot et al., 2006; Derycke et al., 2005; Huang et al., 2005) with conflicting results (Lah et al., 2006). While recently approved antiangiogenic drugs (e.g., bevacizumab) provide grounds for optimism for cancer treatment (Ellis and Kirkpatrick, 2005) the effect of antiangiogenic therapy on length of survival needs further investigation (Bernsen and van der Kogel, 1999; Kuiper et al., 1998). Antiangiogenic treatment can exacerbate hypoxic effects (Steeg, 2003) and cause glioma mass fragmentation,

* Corresponding author.
E-mail address: Vittorio.Cristini@uth.tmc.edu (V. Cristini).
[1] Partial funding from the National Science Foundation, Division of Mathematical Sciences.
[2] Supported in part by NIH-NIGMS RO1 GM47368 (E.L.B.).
[3] Partial funding from the National Science Foundation and National Cancer Institute.
Available online on ScienceDirect (www.sciencedirect.com).

1053-8119/$ - see front matter © 2007 Elsevier Inc. All rights reserved.
doi:10.1016/j.neuroimage.2007.03.008

cancer cell migration, and tissue invasion (Rubenstein et al., 2000; Kunkel et al., 2001; Lamszus et al., 2003; Bello et al., 2004). Similar effects have been recently predicted by computer simulations for some chemotherapies (Sinek et al., 2004).

These variable observations of tumor invasion and response to therapy illustrate the critical need for biologically realistic and predictive multiscale theoretical models that quantitatively connect tumor proliferation and invasion with vascular density, blood flow, and microenvironmental substrate gradients. Indeed, it is clear from experience in the physical sciences that such complex systems, dominated by large numbers of processes and highly nonlinear dynamics, are very difficult to approach by experimental methods alone and can typically be understood only using appropriate mathematical models and sophisticated computer simulations, in addition and complementary to laboratory and clinical observations (Cristini et al., 2006; Sanga et al., 2006). Here we develop a computational (in silico) model whose parameter values and mathematical functions can be informed based on experimental and clinical data to predict tumor prognosis and outcome, including glioma growth, neovascularization, and response to treatment. This method is based on first principles (e.g., diffusion equation) and numerical algorithms that link the tissue scale tumor behavior to the underlying molecular biology by experimentally tested functional relationships between the molecular properties of tumor cells and the environment and tissue scale model parameters. Our central hypothesis is inspired by an engineering approach whereby tumor lesions are viewed as a complex micro-structured material, where the three-dimensional tissue architecture ("morphology") and dynamics are coupled in complex, nonlinear ways to cell phenotype, and this to molecular factors and phenomena in the microenvironment acting both as tumor morphology regulators and as determinants of the invasion potential by controlling the mechanisms of cancer cell proliferation and migration (Friedl and Wolf, 2003) among others.

In our approach, we develop models of Functional Collective Cell-Migration Units (FCCMU) that describe the large-scale morphology and 3D cell spatial arrangements during tumor growth and invasion and incorporate micro–macro functional relationships as described above. This includes the application of mathematical and empirical methods to quantify the competition between cell substrate gradient-related pro-invasion phenomena and molecular forces that govern proliferation and taxis, and forces opposing invasion through cell adhesion. The latter, under normoxic conditions, often enforce compact non-infiltrative tumor morphology while local oxygen gradients promote invasion (Steeg, 2003; Page et al., 1987; Seftor et al., 2002; Kunkel et al., 2001; Pennacchietti et al., 2003; Lamszus et al., 2003; Bello et al., 2004; Rubenstein et al., 2000; Rofstad and Halsor, 2002; DeJaeger et al., 2001; Cristini et al., 2005; Frieboes et al., 2006; Macklin and Lowengrub, 2007). Interactions between cellular proliferation and adhesion and other phenotypic properties may be reflected in both the surface characteristics, e.g., stability, of the tumor–host interface and the growth characteristics of tumors (Cristini et al., 2003, Cristini et al., 2005; Frieboes et al., 2006; Gatenby et al., 2006; Macklin and Lowengrub, 2007). These characteristics give rise to various tumor morphologies and influence treatment outcomes. The model thus enables the deterministic linking of collective tumor cell motion on the balance between cellular properties and the microenvironment. In this paper, we focus on describing the gross morphologic behavior resulting from a typical glioma phenotype. Direct links to the underlying genotype are studied elsewhere (Bearer and Cristini, manuscript submitted).

We assemble this 3D multiscale computational model of cancer as a key step towards the transition from qualitative, empirical correlations of molecular biology, histopathology, and imaging to quantitative and predictive mathematical laws founded on the underlying biology. The model provides resolution at various tissue physical scales, including the microvasculature, and quantifies functional links of molecular factors to phenotype that currently for the most part can only be tentatively established through laboratory or clinical observation. This mathematical and computational approach allows observable properties of a tumor, e.g., its morphology, to be used to both understand the underlying cellular physiology and predict subsequent growth (or treatment outcome), providing a bridge between observable, morphologic properties of the tumor and its prognosis (Cristini et al., 2006; Sanga et al., 2006).

Method overview

The FCCMU model is based on conservation laws (e.g., of mass and momentum) with conserved variables that describe the known determinants of glioma (e.g., cell density) and with parameters that characterize a specific glioma tissue. The conservation laws consist of well established, biologically founded convection–reaction–diffusion equations that govern the densities of the tumor cell species, the diffusion of cytokines, and the concentration of vital nutrients. The model describes the cells' (collective) migratory response and interaction with the extracellular matrix (ECM) and an evolving neovasculature. The collective tumor cell velocity depends on proliferation-driven mechanical pressure in the tissue, chemotaxis and haptotaxis due to gradients of soluble cytokines and insoluble matrix macromolecules. The cell species velocity is obtained from a Darcy's law coarse scale reformulation of the inertialess momentum equation, which is the instantaneous equilibrium among the following forces: pressure, resistance to motion (cell adhesion), elastic forces, forces exchanged with the extracellular matrix (ECM) leading to haptotaxis and chemotaxis, and other mechanical effects (e.g., Cristini et al., 2003, 2005; Zheng et al., 2005; Frieboes et al., 2006; Sanga et al., 2006; Li et al., 2007; Anderson and Chaplain, 1998; Anderson, 2005; Anderson et al., 2000; Chaplain and Lolas, 2005; Adam, 1996; Bellomo and Preziosi, 2000; Chaplain and Anderson, 2003; Friedman, 2004; Araujo and McElwain, 2003; Macklin and Lowengrub, 2005; Greenspan, 1976; Byrne and Chaplain, 1996a,b; Ambrosi and Guana, 2005; Macklin and Lowengrub, 2007; Ambrosi and Preziosi, 2002; Byrne and Preziosi, 2003; Chaplain et al., 2006). Cells produce proteases, which degrade the matrix locally, making room for cells to migrate. In the model, matrix degradation releases cytokines and growth promoters, thus having biological effects on tumor cells (e.g., Chaplain and Anderson, 2003). The model can account for cell–cell interactions (cell–cell adhesion and communications), high polarity, and strong pulling forces exchanged by cells and ECM (Friedl and Wolf, 2003).

The FCCMU model is coupled nonlinearly to a hybrid continuum-discrete, lattice-free model of tumor-induced angiogenesis (Plank and Sleeman, 2003, 2004). The angiogenesis component describes proliferation and migration due to chemotaxis and haptotaxis of endothelial cells in response to tumor angiogenic regulators (e.g., VEGF) and matrix macromolecules, respectively.

The angiogenic regulators are released by perinecrotic tumor cells and host cells near the tumor–host interface (Takano et al., 1996; Shweiki et al., 1999), which stimulate vascular endothelial cells of the brain vasculature to proliferate and begin to form vessels (Jain, 2003). Anastomosed vessels may provide a source of nutrient in the tissue and may undergo spontaneous shutdown and regression during tumor growth (Holash et al., 1999b). We note that there are other related lattice-based models of tumor neovascularization (e.g., Sun et al., 2005; McDougall et al., 2006). Although tumor angiogenesis may occur via the formation of sprouts or intussuception (Patan et al., 2001b), for simplicity here only the former process is incorporated in the model. Input parameter values to the model, e.g., cell proliferation and apoptosis, are estimated from in vitro cell lines and ex vivo patient data. The parameters governing the extent of neovascularization and nutrient supply due to blood flow are estimated in part from Dynamic Contrast Enhanced Magnetic Resonance Imaging (DCE-MRI) observations in patients (O'Connor et al., 2007).

The FCCMU model describes nutrient/oxygen delivery from the neovasculature (via convection and diffusion (Chaplain, 1996; Jain, 2001)) and cellular uptake, and nutrient, oxygen, and growth factor diffusion through the tumor tissue (Byrne and Chaplain, 1997). Oxygen/nutrient availability limits the fraction of cycling cells. Regions of tissue become hypoxic and then necrotic where nutrient/oxygen concentration falls below a threshold. The model describes evolution of local mass fractions of viable tumor species, necrotic and host tissues. Cell mass exchange occurs due to mutations, mitosis, necrosis, and apoptosis. Lysis rates describe the disintegration of tumor cell mass and the radial effusion of fluid away from the necrotic regions. All rates are inverse times (unit time = 1 day).

By solving the nonlinearly coupled FCCMU/angiogenesis equations numerically we predict the combination of variables most likely to lead to growth and invasion, such as nutrient and angiogenic regulator concentrations and diffusion rates; rates of proliferation, apoptosis, and nutrient consumption; genotypic mutations in oncogenes, tumor suppressors, and migration-associated genes. At any given time during tumor growth, the model outputs the computed values of all relevant variables at every location within the three-dimensional tumor tissue, e.g., the spatial distributions of oxygen, nutrients, and tumor cell species. The result is a description of the complex, multi-scalar dynamics of in vivo 3-dimensional tumors through avascular, neovascular, vascular growth, and invasion stages.

Summary of materials and equipment used

Histopathology of human glioma

Four archived autopsied brains obtained from the Brown University-Rhode Island Hospital Brain Bank were examined in hemotoxylin–eosin stained paraffin sections prepared according to standard autopsy procedures. Autopsied diagnosis of glioblastoma multiforme was confirmed by two neuropathologists, and morphology at the tumor margins imaged on a Zeiss AxioImager by standard bright field and by fluorescence using FITC and rhodamine filters. Selective fluorescence in the rhodamine channel of hemoglobin in red blood cells combined with autofluorescence of connective tissue in the FITC channel greatly enhances detection of vasculature patterns in H&E sections of archived material (Bearer, unpublished methodology).

Multiscale model

The minimal formulation of the FCCMU model is based on reaction–diffusion equations that govern a tumor cell density, an evolving neovasculature, a vital nutrient concentration, the ECM, and matrix degrading enzymes. Extensions to include more complex biophysics, e.g., multiple nutrients, growth inhibitors, and matrix remodeling, are straightforward.

In our approach, each constituent moves with its own velocity field; mass, momentum, and energy equations are posed for each constituent. Through experimental comparisons and the inclusion of molecular-scale effects, we formulate functional relationships that close the FCCMU model. Generically, the reaction–diffusion equations take the form

$$v_t = -\nabla \cdot \mathbf{J} + \Gamma_+ - \Gamma_-, \tag{1}$$

where v is the evolving variable, $\mathbf{J}$ is the flux, Γ_+ and Γ_- are the sources and sinks. Letting $v=\rho_i$, σ, f, and m, respectively, be the tumor cell density of species i or host density, the vital nutrient concentration (e.g., oxygen), the (nondiffusible) matrix macromolecule (e.g., fibronectin (Anderson and Chaplain, 1998; Anderson, 2005)), and matrix degrading enzyme, MDE (e.g., matrix metalloproteinases, urokinase plasminogen activators) (Anderson et al., 2000; Anderson, 2005; Chaplain and Lolas, 2005) concentrations, we may take

$$\mathbf{J} = \begin{cases} \rho_i \mathbf{u}_i + \mathbf{J}_{\text{mechanics},i} & \text{if } v = \rho_i \\ \sigma \mathbf{u}_{\text{w}} - D_\sigma \nabla \sigma & \text{if } v = \sigma \\ 0 & \text{if } v = f \\ m \mathbf{u}_{\text{w}} - D_m \nabla m & \text{if } v = m \end{cases},$$

$$\Gamma_+ = \begin{cases} \rho_i \lambda_{\text{prolif},i} + \sum_j S_{ij}^+ & \text{if } v = \rho_i \\ \lambda_{\text{blood}} & \text{if } v = \sigma \\ \lambda_f & \text{if } v = f \\ \lambda_{\text{mde}} & \text{if } v = m \end{cases} \tag{2}$$

$$\Gamma_- = \begin{cases} \rho_i \lambda_{\text{death},i} + \sum_j S_{i,j}^- & \text{if } v = \rho_i \\ \lambda_{\sigma,\text{uptake}} & \text{if } v = \sigma \\ \lambda_{f,\text{degrade}} & \text{if } v = f \\ \lambda_{\text{mde,degrade}} & \text{if } v = m \end{cases}$$

where $\mathbf{u}_i$ is the cell velocity of species/host i, $\mathbf{u}_{\text{w}}$ is the velocity of water (i.e., assuming transport of chemical factors is primarily through the interstitial liquid), the Ds are diffusion constants, and λ_{prolif}, λ_{death}, λ_{blood}, λ_{uptake}, λ_{f}, $\lambda_{\text{f,degrade}}$, λ_{mde}, and $\lambda_{\text{mde,degrade}}$ are the mitosis, apoptosis and necrosis, blood–tissue nutrient transfer, and uptake and decay rates, respectively, for matrix molecules and MDE. An additional equation (not shown) is posed for the mass fraction of water. The flux $\mathbf{J}_{\text{mechanics},i}$ accounts for the mechanical interactions among the different cell species. A major component of the FCCMU model is the development of the constitutive law for $\mathbf{J}_{\text{mechanics},I}$. This is obtained from a variational approach from an energy formulation that accounts for the mechanical forces, e.g., cell–cell and cell–matrix adhesion, and elastic effects (residual stress). A feature of this approach is the incorporation of a novel continuum model of adhesion in this flux. Following the variational approach developed for diffuse interface models of multiphase flows and materials by Lowengrub and coworkers (e.g., Lowengrub and Truskinovsky, 1998;

Leo et al., 1998; Lee et al., 2002; Kim et al., 2004a,b; Wise et al., 2004; Kim and Lowengrub, 2005) and others (e.g., Garcke et al., 2004; Jacqmin, 1999; Anderson et al., 1998) we introduce a continuum model of cell–cell and cell–matrix adhesion energy which can be written as an integral taken over the entire tumor/host domain $E_{\text{adhesion},i} = \int f_i(\rho_1, \ldots, \rho_N) + \frac{1}{2}\sum_{j=1}^{N} \varepsilon_{i,j}^2 |\nabla \rho_j|^2 \mathrm{d}x$. The first term is a bulk energy, which accounts for the degree of miscibility of cell and host species, as directed by experiments. The second term introduces cell–cell adhesion forces that generate a surface tension between the phases and further accounts for intermixing across a diffuse interface of thickness that roughly scales with $\varepsilon_{i,i}$. Typically, the cell adhesion energy enforces phase separation of tumor and host tissues sharing a diffuse interface with thickness 1–100 μm. Under the assumption that tumor cells prefer to stay bonded with each other rather than being in any other configuration, that the cell density is roughly constant and that there is only isotropic stress (pressure p), this reduces, in an asymptotic limit, to the "jump" boundary condition $[p]=\tau\kappa$ where τ measures the affinity and κ is the total curvature of the interface (Wise et al., Frieboes et al., manuscripts submitted). This is akin to surface tension in multiphase flows and can also be used to describe tumor encapsulation by ECM fragments and is characteristic of collective cell migration (Friedl and Wolf, 2003).

A thermodynamically consistent constitutive law for the flux $\mathbf{J}_{\text{mechanics},i}$ is obtained by taking the gradient of the variational derivative of the total energy: $\mathbf{J}_{\text{mechanics},i} \propto \nabla(\delta E_{\text{mechanics},i}/\delta\rho_i)$, where $E_{\text{mechanics},i}$ is obtained by adding the contributions from each mechanism modeled, i.e., adhesion, elasticity, etc. The velocities $\mathbf{u}_i$ and $\mathbf{u}_w$ are determined from momentum equations. For example, following previous approaches (e.g., Cristini et al., 2003, 2005; Zheng et al., 2005; Frieboes et al., 2006; Li et al., 2007; Macklin and Lowengrub, 2005, 2007) that are reformulations and generalizations of models in (Greenspan, 1976; Byrne and Chaplain, 1996a,b; Adam, 1996; Bellomo and Preziosi, 2000; Chaplain and Anderson, 2003) and neglecting viscoelastic effects, we take Darcy's law as a coarse scale reformulation of the inertialess momentum equation, which is the instantaneous equilibrium among the following forces: pressure, resistance to motion, elastic forces, forces exchanged with the ECM leading to hapto- and chemotaxis, and other mechanical effects within $E_{\text{mechanics}}$ as discussed above. This leads to

$$\mathbf{u}_i = -M_i \nabla p + \gamma_i(\delta E_{\text{mechanics},i}/\delta\rho_i)\nabla\rho_i + \chi_{f,i}\nabla f + \chi_{\sigma,i}\nabla\sigma \qquad (3)$$

where p is the pressure (isotropic stress) and M_i, γ_i, χ_f and χ_σ are the spatially inhomogeneous mobility, mechano-, hapto-, and chemotaxis tensors that also take into account cell–matrix adhesion. The parameter M_i depends on the extent of cell-to-cell and cell-to-ECM adhesion in bulk regions. Since a number of different parameters in the model describe various effects of cell–cell and cell–ECM adhesion it is expected that this model should have enough complexity to reproduce nontrivial and non-monotonic dependences of migration on CAMs (Friedl and Wolf, 2003). Note that other models such as Stokes, viscoelastic, and nonlinear-elastic/plastic can be incorporated as required.

The FCCMU continuum-scale convection–reaction–diffusion equations are solved numerically using a novel adaptive finite-difference method (Wise et al., Frieboes et al., manuscripts submitted). This method features an adaptive, block-structured Cartesian mesh refinement algorithm (e.g., Berger and Colella, 1989), centered differences in space, and an implicit time discretization for which there is no stability constraint on the space and time steps. The nonlinear equations at the implicit time level are solved efficiently using a multilevel, nonlinear multigrid method (e.g., Brandt, 1977). A typical simulation (e.g., Fig. 1) required two days of CPU time on a Xeon processor with 3.06 GHz and 2 GB of RAM.

Tumor vasculature

We model the physiology and evolution of glioma neovasculature in 3D using a hybrid continuum-discrete, lattice-free model of tumor angiogenesis which is a refinement of earlier work (Plank and Sleeman, 2003, 2004). This was shown to create dendritic structures consistent with experimentally observed tumor capillaries (Less et al., 1991; Skinner, 1990). This random-walk model generates vascular topology based on tumor angiogenic regulators, e.g., vascular endothelial growth factor (VEGF) (Takano et al., 1996), represented by a single continuum variable that reflects the excess of pro-angiogenic regulators compared to inhibitory factors. Peri-necrotic tumor cells and host tissue cells close to the tumor boundary are assumed to be a source of angiogenic regulators (e.g., VEGF). Endothelial cells near the sprout tips proliferate and their migration is described by chemotaxis and haptotaxis (e.g., motion up gradients of angiogenic regulators and matrix proteins such as fibronectin). For simplicity, only leading endothelial cells are modeled and trailing cells passively follow. The vasculature architecture, i.e., interconnectedness and anastomoses, is captured via a set of rules, e.g., a leading endothelial cell has a fixed probability of branching at each time step while anastomosis occurs if a leading endothelial cell crosses a vessel trailing path. Glioma vessels are more tortuous than normal vessels (Bullitt et al., 2005). This can be quantified by various means including a "Sum of Angles Metric" (SOAM) that sums total curvature along a space curve and normalizes by path length, indicating high frequency, low-amplitude sine waves or coils (Bullitt et al., 2005).

The tumor-induced vasculature does not initially conduct blood as the vessels need to form loops first (anastomosis) (Augustin, 2001). As observed experimentally, the neovasculature model may also account for increasing vessel diameters and spontaneous shutdown and consecutive regression of initially functioning tumor vessel segments or whole microvascular areas (Holash et al., 1999b). Here, functional anastomosed vessels were assumed to provide a source of nutrient in the tissue proportionally to local pressure.

Calculation of model parameters

Previous measurements of growth and histology of in vitro ACBT (human glioblastoma multiforme) tumor spheroids (Frieboes et al., 2006) and of human glioma (Bearer and Cristini, manuscript submitted) were used to inform the parameters of the simulation presented herein. Briefly, higher-grade glioma mitosis and apoptosis rates were taken to be 1 day^{-1} and 0.32 day^{-1} respectively. The characteristic time scale was taken to be the inverse mitosis rate. The diffusion penetration length was measured to be 100 μm (Cristini et al., 2003; Frieboes et al., 2006) and is used herein as the characteristic unit of length. The necrosis threshold was taken to be $\sigma_N/\sigma_V=0.5$, where σ_N is the nutrient concentration needed for viability and σ_V is the nutrient concentration in the far-field. Mutation rates from low- to high-

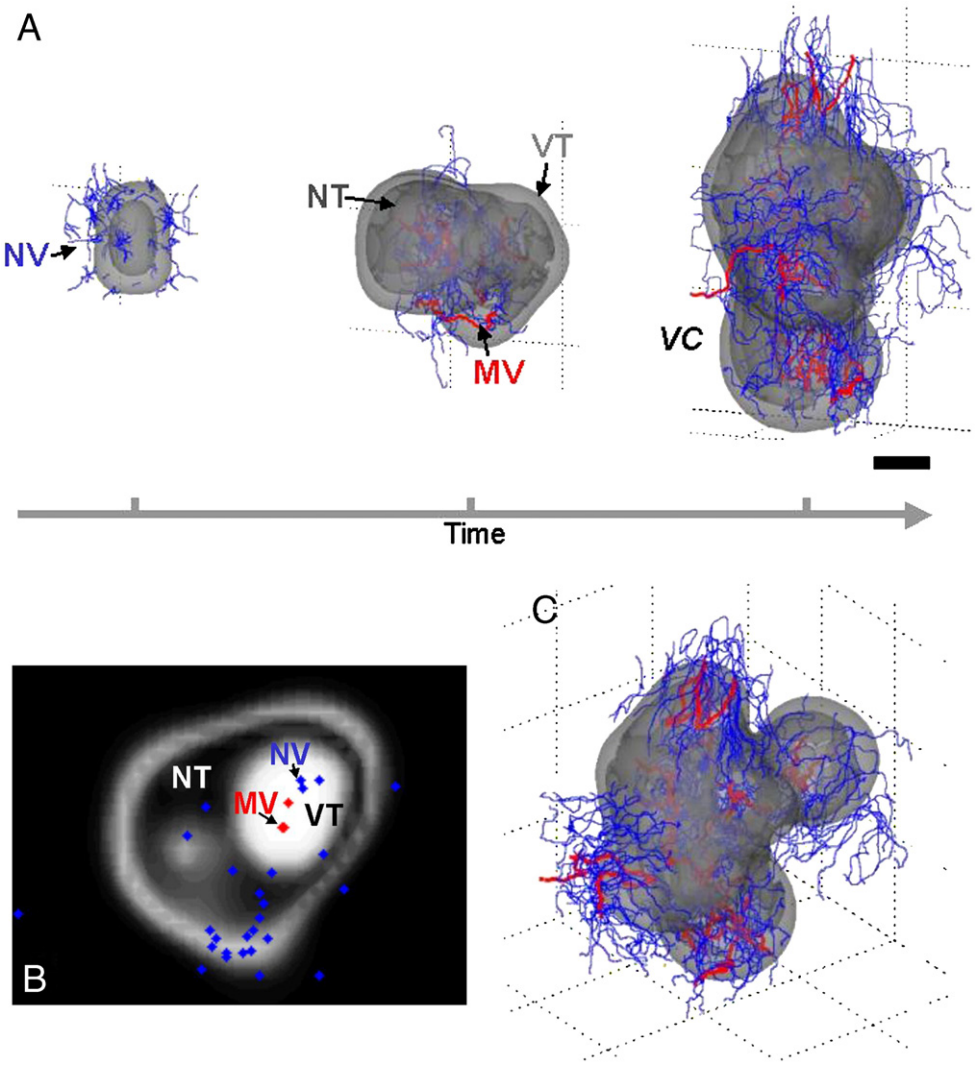

Fig. 1. Multiscale 3D computer model predicts gross morphologic features of a growing glioblastoma. (A movie of this simulation is in the Supplementary data.) (A) Viable (VT) and necrotic (NT) tissue regions and vasculature (MV: mature blood-conducting vessels in red; NV: new non-conducting vessels in blue) are shown. The time sequence (from left to right, over a period of 3 months) reveals that the morphology is affected by successive cycles of neovascularization, vasculature maturation, and vessel cooption (VC). Scale bar, 250 μm. (B) Histology-like section of the last frame of the simulation in A (obtained by slicing horizontally through the simulated tumor) reveals viable tumor regions (white) surrounding necrotic tissue (dark). Tumor mass spatial distribution is calculated using Eq. (1) with $v=\rho$ and cell viability as a function of nutrient concentration \sigma, calculated using Eq. (1) with $v=\sigma$. Input parameters were calibrated from in vitro and ex vivo glioma data (Summary of materials and equipment used). In particular, tumor cells are estimated to proliferate at a rate $\lambda_{prolif}=1$ day^{-1} (Frieboes et al., 2006). (C) Another view from simulation shown in panel A, right.

grade glioma were also estimated in previous work (Bearer and Cristini, manuscript submitted) but not utilized here. In previous work, a critical value of cell adhesion parameter was determined from shape stability analysis of experimental and simulated spheroids (Frieboes et al., 2006): compact spherical morphologies exist only for sufficiently large adhesion, which is implemented via the parameter γ_i (after non-dimensionalization) in Eq. (3). The above set of parameters provided the baseline for our simulations (Fig. 1 shows a simulation using a sub-critical value of the adhesion parameter). Simulations were performed using one fixed set of parameters as described above. Parameter sensitivity studies were performed where cell adhesion (γ_i) and cell chemotaxis ($\chi_{\sigma,i}$) parameters were varied to study their effect on the morphology of infiltrating collective-cell patterns (i.e., cell chains vs. strands vs. detached clusters (Friedl and Wolf, 2003)). Representative resulting morphologies are reported elsewhere (Sanga et al., 2007) and confirm that for relatively low cell adhesion morphologic instability occurs when nutrient heterogeneity is present leading to the development of infiltrative cell protrusions (Cristini et al., 2003; Frieboes et al., 2006; Macklin and Lowengrub, 2007; Bearer and Cristini, manuscript submitted). The shape features of these protrusions further depend on the relative strengths of cell proliferation and cell chemotaxis. A control was provided by simulations corresponding to relatively high cell adhesion, for which tumors grow spherical and morphologic instability does not occur.

Complex tissue structure

To model complex tissue structures, an additional variable S is introduced to model the local structure of the tissue. For example,

in the simulation described below, we take $S=1$ where there is bone (e.g., cranium). We then take the mobility, mechano-, hapto-, and chemotaxis tensors M, γ_i, χ_f and χ_σ to be spatially inhomogeneous such that that these tensors (assumed to be isotropic in the simulation below) are small in regions where S is approximately equal to 1.

Results

The 3D multiscale model correctly predicts gross morphologic features of growing tumors (Fig. 1). (A movie of this simulation is in the Supplementary data.) Fig. 1A shows a mm-sized glioblastoma during early stages of growth simulated using our 3D multiscale model. The model predicts regions of viable cells, necrosis in inner tumor areas, and a tortuous neovasculature as observed in vivo (Bullitt et al., 2005). The vessels labeled in red are capable of releasing nutrient. The rate of nutrient released may depend on their age and the solid pressure in the tissue. The vessels migrate towards the tumor/host interface since peri-necrotic tumor cells and host tissue cells close to the tumor boundary are assumed to produce angiogenic factors and other regulators. The tumor eventually coopts and engulfs the vessels. The tumor-induced vasculature does not initially conduct blood as the vessels need to form loops first (anastomosis) (Augustin, 2001), i.e., more mature vessels that have anastomosed conduct blood and may release nutrient. By hypothesizing the underlying mechanisms driving these phenomena, the model enables a quantitative analysis, e.g., viable region thickness of about 100–200 μm and extent of necrosis as seen in Fig. 1B are shown to be strongly dependent on diffusion gradients of oxygen/nutrient in the microenvironment and agree with previous experiments (Helmlinger et al., 1997; Frieboes et al., 2006). Chaotic angiogenesis leads to heterogeneous perfusion in the tumor that then might be responsible for regression of parts of the vascular network and necrosis of tumor cells (Carmeliet and Jain, 2000; Patan et al., 2001b), further enhancing variable tumor cell proliferation. By taking vessel maturation into account, the simulations correctly predict that, as tumor size increases, inner vessels may regress or shut down, leading to nutrient depletion and resulting in the formation of a large necrotic core (data not shown), as observed in patients. For example, cm-sized human glioblastoma at later stages as seen through magnetic resonance imaging (MRI) in patients (e.g., Wurzel et al., 2005) is composed of viable cells delineating its boundary and surrounding extensive necrosis in its inner region.

The multiscale model enables the prediction of tumor morphology by quantifying the spatial diffusion gradients of cell substrates maintained by heterogeneous cell proliferation and an abnormal, constantly evolving vasculature. Figs. 1A and C show a simulated time sequence over the course of 3 months predicting that the glioblastoma grows with a thin layer of viable tissue on its periphery, displacing nearby tissue and internally generating necrosis. The morphology is directly influenced by angiogenesis, vasculature maturation, and vessel cooption (Vajkoczy et al., 2002; Augustin, 2001; Holash et al., 1999a). The model predicts that the tumor boundary moves at a rate of about 50–100 μm per week, presenting a mass of diameter of about 5 cm in 1 year (data not shown). These results are supported by well-known clinical observations (e.g., Naganuma et al., 1989). As the tumor grows and engulfs vessels in its vicinity, the tumor may compress the vessels (Padera et al., 2004) and disrupt flow of nutrients, leading to further necrosis and even temporary mass and vascular regression (Zagzag et al., 2000; Holash et al., 1999b). The crucial role of cell substrate gradients on tissue structure and tumor invasion is further analyzed below (Figs. 2 and 3). Fig. 1B shows a histology-like section of the last frame of the simulation in Fig. 1A, obtained by slicing horizontally through the simulated tumor. Viable tumor regions (white) surround necrotic tissue (dark), as seen in vivo in MRI (e.g., Wurzel et al., 2005) and ex vivo in histopathology (see below).

A growing tumor contends with increasing mechanical resistance from normal brain tissue, which has physical properties resembling a gel (Ommaya, 1968; Fallenstein et al., 1969). Nevertheless, this resistance is insufficient to contain tumor growth, e.g., gliomas have been observed to displace cartilage (Kumar et al., 2003). Only hard bone (e.g., the skull) will be a physical barrier. The effect of such physical barriers on tumor morphology and growth can be incorporated in the multiscale model (see Summary of materials and equipment used).

In the attached movie, we simulate an aggressive tumor growing in a 1.3 cm^2 of brain tissue (upper left frame), which includes white matter (lightest gray), gray matter (medium gray), bone (white), external blood vessels (darkest gray), and fluid (black) in the folds of the cerebral cortex. As the tumor grows, oxygen levels drop (upper right frame), leading to hypoxia (blue regions in upper left frame), the secretion of pro-angiogenic growth factors (lower right frame), and necrosis (brown regions in the upper left frame).

The tumor response to oxygen availability leads to pressure variations. During the early period of rapid growth, pressure increases in the tumor and the surrounding tissue. Later, volume loss in the necrotic core moderates the pressure. (See day 10.) The inhomogeneous necrotic volume loss leads to morphological instability, seen in the formation of rapidly developing buds that invade the surrounding tissue and increase the pressure. (See days 20 to 30.) Thereafter, we see a cyclic pattern of rapid proliferation and pressure buildup followed by necrosis-induced pressure relief. The tissue geometry plays a critical role in this process. Tumor buds invading the white matter (top of the tumor) encounter less mechanical resistance, leading to the formation of relatively slender invasive fingers, compared to the blunt bulbs invading the gray matter. The tumor buds also rapidly elongate and grow along the folds of the cortex where the tumor cells are highly mobile. As the tumor continues to grow, pressure builds between the tumor and the cranium, which retards the growth of the tumor towards the skull in spite of ample oxygen and nutrients (top right frame).

Tumor structure and morphology are significantly affected by diffusion gradients, e.g., of oxygen and nutrients, in the cellular microenvironment (Fig. 2). The computer model (histology-like sections of the last frame of the simulation in Fig. 1A, obtained by slicing vertically through the simulated tumor) predicts that viable regions of thickness of about 100–200 μm encircle the neo-vessels (Kunkel et al., 2001), with acellular (necrotic) areas in between them, thereby determining the tumor tissue architecture (Fig. 2A) based on the diffusion limit for cell substrates (Fig. 2B) (Helmlinger et al., 1997). As a consequence, overall tumor shape is also determined by the distribution of vessels (Fig. 2A). These results are supported by numerous experimental observations in animal glioblastoma models (Rubenstein et al., 2000; Kunkel et al., 2001; Lamszus et al., 2003; Bello et al., 2004), and from histopathology of brain tumors in patients, and may also apply to solid tumors in general (Cristini et al., 2005; Frieboes et al., 2006) beyond the context of brain tumors. A histology section of glioblastoma from a

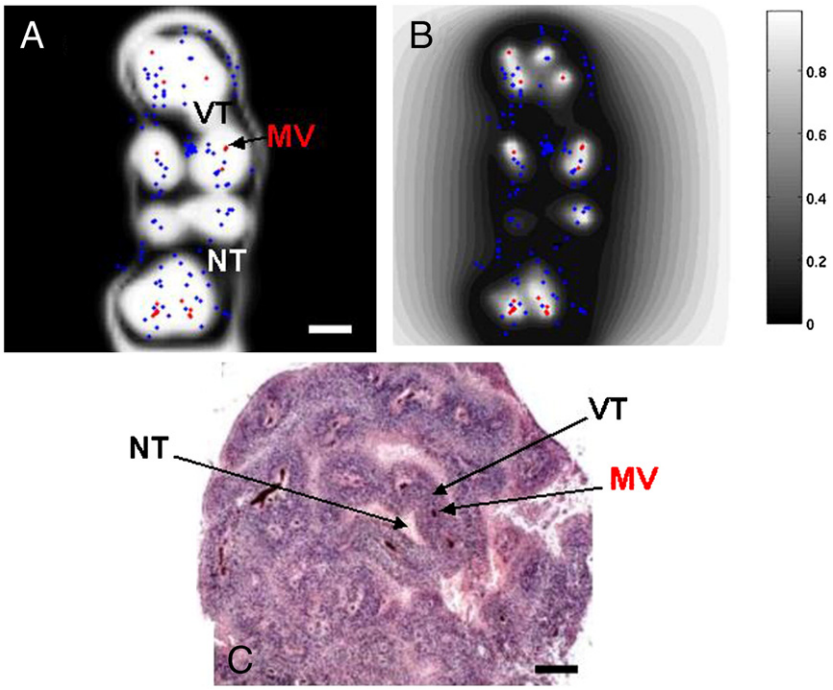

Fig. 2. Multiscale model predicts that tumor tissue morphology is determined by diffusion gradients. (A) Tumor histology predicted by the computer model (obtained by slicing vertically through the simulated tumor corresponding to last frame in panel A) reveals clusters of viable cells (VT) surrounding blood vessel cross-sections (MV), and zones depleted of cells or necrotic farther away (NT). Viable tissue is confined within 100–200 μm of the conducting intra-tumoral vessels and of the brain parenchyma (cross-sections of conducting vessels are in red, non-conducting in blue). Scale bar, 200 μm. (B) Calculated diffusion gradients of cell substrates corresponding to the tumor structure predicted by the simulation in panel A indicate high nutrient (white) in the vicinity of blood conducting vessels and low nutrient (black) otherwise, thereby determining the regions of cell viability. Legend: arbitrary units. (C) Glioblastoma histologic section from a patient shows tissue structure of a large bulb-shaped tumor area. This morphology reveals viable cells (VT) cuffing and surrounding blood vessels in cross-sections (MV), and depleted inter-vessel zones (NT). The thickness of the cuff of viable cells corresponds to the diffusion gradient of oxygen and nutrients they require emanating from the vessel. These results indicate that tumor architecture in this specimen is *determined* by cellular metabolism and intra-tumoral diffusion gradients of required nutrients provided by the vasculature, also confirming the presence of substrate gradients and the parameter estimates for diffusion length used in the simulations (Summary of materials and equipment used). Scale bar, 200 μm.

patient (Fig. 2C) reveals a bulb-shaped group of cells with evident internal vascularization and tissue structure that supports the predictions of the computer model (Figs. 2A, B). Note that overall computed tumor shape (Fig. 2A) is different from that in the patient (Fig. 2C) as the tumor shapes are dictated by the (relatively random) distribution of vessels. However, the internal tissue structures of the computed and in vivo tumors are similar as set by (deterministic) diffusion gradients of cell substrates.

The computer model predicts that substrate diffusion gradients strongly affect tumor invasion in addition to tumor and host tissue morphology and structure (Fig. 3). In silico histopathology of a computer simulation shows that glioma cells may rely on vessels beyond the tumor boundary — and grow towards blood vessels in the host tissue that they contribute to stimulate (Fig. 3A) (Bartels et al., 2006; Preusser et al., 2006). The simulation illustrates an invasive front of tumor cells collectively moving up towards the neovasculature, revealing the dramatic effect of cell substrate gradients on the tumor morphology and invasion beyond molecular-scale signaling events (Tysnes and Mahesparan, 2001). The dynamics of this invasion mechanism, termed "diffusional instability," have been studied elsewhere (Cristini et al., 2003, 2005; Frieboes et al., 2006; Macklin and Lowengrub, 2007). Representative histologic sections from four examples of glioblastoma multiforme in patients also reveal protruding fronts of cells in collective motion away from necrotic areas, up gradients of cell substrates, into areas of the brain where neovascularization is evident and strongly resembling tumor boundary morphologies predicted by the computer simulations. Fig. 3B,C provide a more detailed image of a glioblastoma histology section from a patient that reveals a tumor front (bottom) pushing into the healthy brain tissue (top). Normal brain (white matter) has fewer cell bodies and more abundant amorphous matrix. Invading malignant astrocytes (in the middle) have pleiomorphic nuclei and an irregular distribution. Note clearly demarcated margin between tumor and normal brain tissue, as well as green fluorescent outlines of more mature vascular channels deeper in the tumor. Neovascularization at the tumor–brain interface is readily detected by red fluorescence from erythrocytes inside the vessels. These vessels generate substrate diffusion gradients across the tissue, which in turn drive collective tumor cell infiltration into the brain. More mature vessels within the tumor may be compressed which may restrict the blood flow. Here this is shown by relative lack of red fluorescence from RBCs in the deeper tumor vessels as compared to the vessels in the brain at the tumor margin. This, together with vessel aging, may also reduce the vessel permeability for nutrient/oxygen exchange between the vessels and the tissue (Padera et al., 2004), further promoting substrate gradients pointing outwards from the tumor mass.

Fig. 4 shows the anatomic features of the tortuous tumor vasculature as simulated by the multiscale model (Fig. 4A) and as seen in vivo (Bullitt et al., 2005) (Fig. 4B), enabling both

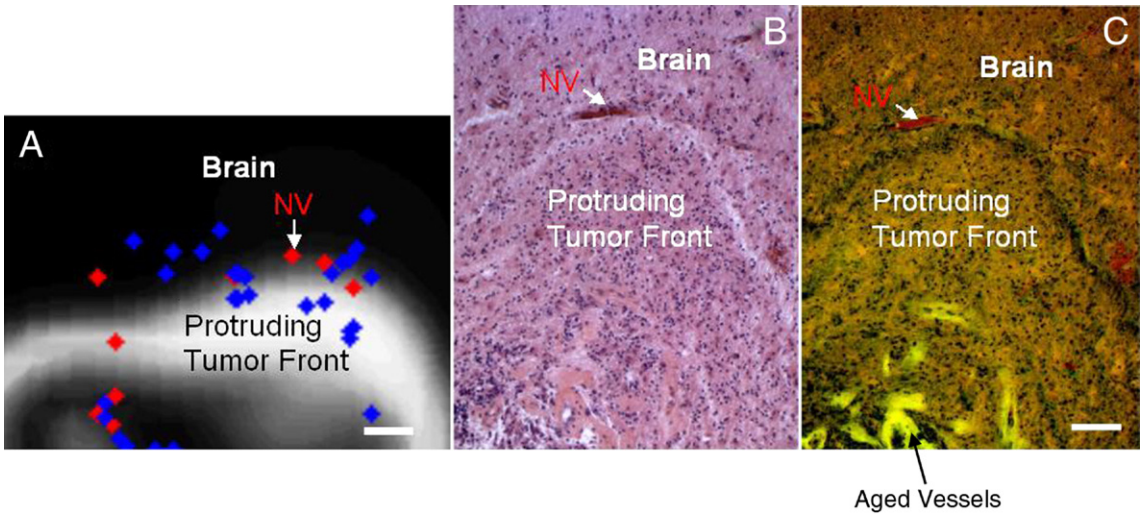

Fig. 3. Multiscale model predicts that tumor tissue invasion is driven by diffusion gradients. (A) Detail of computer simulated glioma histology (obtained by slicing through the 3D simulated tumor of Fig. 1) showing invasive tumor front (white) moving up towards extra-tumoral conducting neo-vessels (NV), supporting the hypothesis that diffusion gradients of cell substrates released by the neovasculature drive collective tumor cell infiltration into the brain in addition to determining the tumor structure (Fig. 2). The model predicts that the movement of tumor fronts towards sources of cell substrate strongly influences glioma invasiveness. Aged vessels inside the tumor have thicker walls and thus are assumed to provide fewer nutrients than the thin-walled neovasculature at the tumor periphery (Padera et al., 2004). Conducting vessels (red), non-conducting (blue). Scale bar, 100 μm. (B and C) Glioblastoma histopathological sections from one patient stained for H&E and viewed by bright field (B) and fluorescence (C) microscopy. Sections show tumor (bottom) pushing into more normal brain (top). Note demarcated margin between tumor and brain parenchyma to the middle top of the image and green fluorescent outlines of large vascular channels deeper in the tumor (C). Neovascularization (NV) at the tumor–brain interface can be detected by red fluorescence from the erythrocytes inside the vessels (see Method overview for microscopic imaging of archived tissue in H&E by fluorescence). Scale bar, 100 μm.

qualitative and future quantitative analyses. In the model, the vasculature structure, e.g., tortuosity and tumor vessel location, is influenced by intermittent tumor tissue hypoxia coupled to both endothelial and tumor cell chemo-and haptotaxis as a function of diffusion gradients of growth factors and other substances in the microenvironment (Li et al., 2000; Bullitt et al., 2005).

Discussion

We have performed, for the first time to our knowledge, 3D computer simulations of growing glioma and neovascular morphologies as predicted by a multiscale mathematical model based on first principles and informed by experimental and clinical data, e.g., histopathology data transformed into model input parameters, and calibrated so that tumor morphology can be predicted beyond a purely empirical, observational approach. Results of glioma morphology, growth, and vascularization obtained through the model are also supported by previous experimental and in vivo studies. Although high-grade gliomas are highly angiogenic and this characteristic correlates with clinical progression (Boegler and Mikkelsen, 2003), microvascular inadequacy may induce necrosis, drive glioma cells to aggressively invade adjacent tissue in vivo

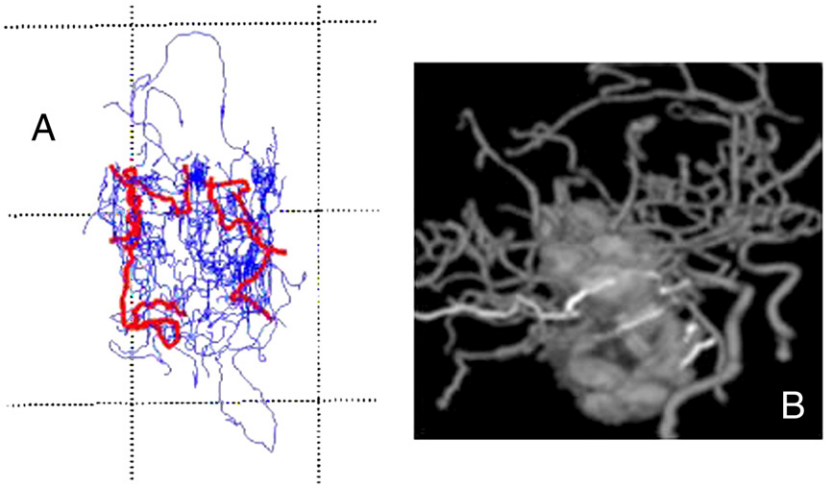

Fig. 4. Anatomic features of glioma vasculature predicted by a simulation (A), highlighting the tortuous nature of the tumor vessels (conducting vessels in red, non-conducting in blue), and observed in vivo (adapted with permission from Bullitt et al. (2005)) (B). The multiscale model predicts that the vasculature is heavily influenced by diffusion gradients of cell substrates driving heterogeneous tumor cell proliferation and concomitant expression of angiogenic regulators.

(Vajkoczy et al., 2002), and trigger angiogenic sprouting from the surrounding microvasculature (as seen in the simulation in Fig. 1A, left). By the second week after implantation in an animal model, gliomas had established their own vasculature and were maintaining it through continued angiogenic sprouting from both host and tumor vessels (Vajkoczy et al., 2002), as is also observed with other tumors (Li et al., 2000). Although some cells showed a strong affinity for the perivascular space of host vessels, the bulk of the tumor did not move towards cerebral vessels. Within 1 week, adjacent host vessels lost the brain–blood barrier, dilated, increased in tortuosity, and produced vascular sprouts, which penetrated the tumor mass and formed the initial tumor neovasculature, in agreement with our results (Fig. 1A, middle). The computer model can accommodate the increase in new tumor vessel diameter (about 1.5×) during a period of 2 weeks, as seen in vivo (Vajkoczy et al., 2002). The model implements a tumor vessel maturation period of 3 weeks that agrees with common physiological models of vessel formation (Cai et al., 2004; Patan et al., 2001a; Cursiefen et al., 2003) and hypothesizes that an evolving vasculature will affect a growing tumor through heterogeneous perfusion (Bernsen et al., 1995), vascular network regression, and tumor cell necrosis, based on in vivo observations (Patan et al., 2001b). The neovasculature is chaotic, of heterogeneous angio-architecture, and has large caliber vessels and sluggish blood flow. While undergoing constant remodeling, the neovasculature is also characterized by spontaneous shutdown and consecutive regression of initially functioning tumor vessel segments or whole microvascular areas, thus maintaining strong diffusion gradients in the microenvironment and directly affecting tumor morphology. This effect is dramatically seen through the model in Fig. 1A, right and Fig. 1C. In this scenario, the tumor grows avascularly first, either coopts the existing vasculature or forms a new one, and then becomes necrotic as this vasculature undergoes regression, leading to new cycles of angiogenesis and growth. Vascular regression associated with the onset of necrosis in the tumor, followed by further angiogenesis at the tumor margins, was also observed experimentally (Holash et al., 1999b).

The multiscale model predicts that glioma tissue structure and tumor invasiveness are significantly influenced by diffusion gradients in the microenvironment, as observed experimentally (Rubenstein et al., 2000; Kunkel et al., 2001; Lamszus et al., 2003; Bello et al., 2004; Frieboes et al., 2006) and in human patients (Bearer and Cristini, manuscript submitted). These gradients may have a strong effect on glioma morphology (Cristini et al., 2005; Macklin and Lowengrub, 2007) and are hypothesized in the model to reciprocally influence a growing tumor's continuously evolving vasculature in complex ways. The 3D model facilitates this study by calculating the chemotactic and haptotactic response of the blood vessels at the cell scale (see Summary of materials and equipment used) and its cumulative effect at the tumor scale (Fig. 4A).

Glioma invasion introduces barriers to tumor resection and to therapy, and even when resection is an option, accurate prediction of the lesion's invasive potential could help decide on a case-by-case if resection is indeed the best option and the optimal volume of lesion to be removed, thus directly impacting the grim outlook of this disease. The multiscale model proposed herein could be of benefit to develop novel intervention strategies and better understand current ones. By modeling tumor behavior in response to chemotherapeutic drugs whose target is known, outcomes may be predicted for individual patients. In addition, experiments in silico using this modeling algorithm may serve as test-beds for drug development thereby avoiding any need initially for clinical efficacy testing in humans. Furthermore, because the underlying molecular and cellular biology are complex, the targets available for intervention strategies and their combinations are virtually infinite. The parameter space can be searched using the mathematical model to identify critical parameters or combinations of parameters to sharpen the experimental focus (Cristini et al., 2006). The advanced state of this modeling technology, coupled with the availability of high performance computing, enables us to propose that it is time to start integrating and further develop this methodology with therapeutic practice.

Acknowledgments

VC very gratefully acknowledges Robert Gatenby (Radiology, University of Arizona) for help in understanding the clinical implications of the quantification of the links of morphology with phenotype and invasion. The authors gratefully acknowledge Sandeep Sanga (Biomedical Engineering, University of California, Irvine) for helpful comments and discussions. The authors thank Ed Stopa at Rhode Island Hospital and the Columbia University Alzheimer's Brain Bank for archived human glioma specimens.

Appendix A. Supplementary data

Supplementary data associated with this article can be found, in the online version, at doi:10.1016/j.neuroimage.2007.03.008.

References

Adam, J., 1996. General aspects of modeling tumor growth and the immune response. In: Adam, J., Bellomo, N. (Eds.), A Survey of Models on Tumor immune Systems Dynamics. Birkhauser, Boston, pp. 15–87.

Ambrosi, D., Guana, F., 2005. Stress-modulated growth. Math. Mech. Solids. doi:10.1177/1081286505059739.

Ambrosi, D., Preziosi, L., 2002. On the closure of mass balance models for tumor growth. Math. Models Methods Appl. Sci. 12, 737–754.

Anderson, A.R.A., 2005. A hybrid mathematical model of solid tumor invasion: the importance of cell adhesion. Math. Med. Biol. 22, 163–186.

Anderson, A.R.A., Chaplain, M.A.J., 1998. Continuous and discrete models of tumour-induced angiogenesis. Bull. Math. Biol. 60, 857–899.

Anderson, D.M., McFadden, G.B., Wheeler, A.A., 1998. Diffuse interface methods in fluid mechanics. Annu. Rev. Fluid Mech. 30, 139–165.

Anderson, A.R.A., Chaplain, M.A.J., Newman, E.L., Steele, R.J.C., Thompson, A.M., 2000. Mathematical modeling of tumour invasion and metastasis. J. Theor. Med. 2, 129–154.

Araujo, R.P., McElwain, D.L.S., 2003. A history of the study of solid tumor growth: the contribution of mathematical modeling. Bull. Math. Biol. 66, 1039–1091.

Augustin, H.G., 2001. Tubes, branches, and pillars. The many ways of forming a new vasculature. Circ. Res. 89, 645–647.

Bartels, U., Hawkins, C., Jing, M., Ho, M., Dirks, P., Rutka, J., Stephens, D., Bouffet, E., 2006. Vascularity and angiogenesis as predictors of growth in optic pathway/hypothalamic gliomas. J. Neurosurg. 104, 314–320.

Bello, L., Lucini, V., Costa, F., Pluderi, M., Giussani, C., Acerbi, F., Carrabba, G., Pannacci, M., Caronzolo, D., Grosso, S., Shinkaruk, S., Colleoni, F., Canron, X., Tomei, G., Deleris, G., Bikfalvi, A., 2004. Combinatorial administration of molecules that simultaneously inhibit angiogenesis and invasion leads to increased therapeutic efficacy in mouse models of malignant glioma. Clin. Cancer Res. 10, 4527–4537.

Bellomo, N., Preziosi, L., 2000. Modeling and mathematical problems related to tumor evolution and its interaction with the immune system. Math. Comp. 413–452.

Berger, M., Colella, P., 1989. Local adaptive mesh refinement for shock hydrodynamics. J. Comp. Phys. 82, 64–84.
Bernsen, H.J.J.A., van der Kogel, A.J., 1999. Antiangiogenic therapy in brain tumor models. J. Neuro-oncol. 45, 247–255.
Bernsen, H.J.J.A., Rijken, P.F.J.W., Oostendorp, T., van der Kogel, A.J., 1995. Vascularity and perfusion of human gliomas xenografted in the athymic nude mouse. Br. J. Cancer 71, 721–726.
Boegler, O., Mikkelsen, T., 2003. Angiogenesis in glioma: molecular mechanisms and roadblocks to translation. The Cancer Journal 9, 205–213.
Brandt, A., 1977. Multi-level adaptive solutions to boundary-value problems. Math. Comput. 31, 333–390.
Bullitt, E., Zeng, D., Gerig, G., Aylward, S., Joshi, S., Smith, J.K., Lin, W., Ewend, M.G., 2005. Vessel tortuosity and brain tumor malignance: a blinded study. Acad. Radiol. 12, 1232–1240.
Byrne, H.M., Chaplain, M.A.J., 1996a. Growth of necrotic tumors in the presence and absence of inhibitors. Math. Biosci. 135, 187–216.
Byrne, H.M., Chaplain, M.A.J., 1996b. Modeling the role of cell–cell adhesion in the growth and development of carcinomas. Math. Comput. Model. 24, 1–17.
Byrne, H.M., Chaplain, M.A.J., 1997. Free boundary value problems associated with the growth and development of multicellular spheroids. Eur. J. Appl. Math. 8, 639–658.
Byrne, H.M., Preziosi, L., 2003. Modeling solid tumor growth using the theory of mixtures. Math. Meth. Biol. 20, 341–366.
Cai, W.-J., Scholz, D., Ziegelhoeffer, T., 2004. Structural remodeling during growth of collateral vessels. In: Schaper, W., Schaper, J. (Eds.), Arteriogenesis. Kluwer Academic Publishers, Boston.
Carmeliet, P., Jain, R.K., 2000. Angiogenesis in cancer and other diseases. Nature 407, 249–257.
Chaplain, M.A.J., 1996. Avascular growth, angiogenesis and vascular growth in solid tumours: the mathematical modelling of the stages of tumour development. Math. Comput. Model. 23, 47–87.
Chaplain, M.A.J., Anderson, A.R.A., 2003. Mathematical modeling of tissue invasion. In: Preziosi, L. (Ed.), Cancer Modeling and Simulation. CRC Press, pp. 269–297.
Chaplain, M.A.J., Lolas, G., 2005. Mathematical modeling of cancer cell invasion of tissue: the role of the urokinase plasminogen activation system. Math. Models Methods Appl. Sci. 15, 1685–1734.
Chaplain, M.A.J., Graziano, L., Preziosi, L., 2006. Mathematical modeling of the loss of tissue compression responsiveness and its role in solid tumor development. Math. Med. Biol. 23, 192–229.
Condeelis, J., Singer, R.H., Segall, J.E., 2005. The great escape: when cancer cells hijack the genes for chemotaxis and motility. Annu. Rev. Cell Dev. Biol. 21, 695–718.
Cristini, V., Lowengrub, J., Nie, Q., 2003. Nonlinear simulation of tumor growth. J. Math. Biol. 46, 191–224.
Cristini, V., Frieboes, H.B., Gatenby, R., Caserta, S., Ferrari, M., Sinek, J.P., 2005. Morphological instability and cancer invasion. Clin. Cancer Res. 11, 6772–6779.
Cristini, V., Gatenby, R., Lowengrub, J., 2006. Multidisciplinary studies of tumor invasion and the role of the microenvironment. NIH 1R01CA127769-01.
Cursiefen, C., Hofmann-Rummelt, C., Kuechle, M., Schloetzer-Schrehardt, U., 2003. Pericyte recruitment in human corneal angiogenesis: an ultrastructural study with clinicopathological correlation. Br. J. Ophtalmol. 87, 101–106.
DeJaeger, K., Kavanagh, M.-C., Hill, R., 2001. Relationship of hypoxia to metastatic ability in rodent tumours. Br. J. Cancer 84, 1280–1285.
Derycke, L., Van Marck, V., Depypere, H., Bracke, M., 2005. Molecular targets of growth, differentiation, tissue integrity, and ectopic cell death in cancer cells. Cancer Biother. Radiopharm. 20, 579–588.
Eble, J.A., Haier, J., 2006. Integrins in cancer treatment. Curr. Cancer Drug Targets 6, 89–105.
Ellis, L.M., Kirkpatrick, P., 2005. Bevacizumab. Nat. Rev., Drug Discov. 4, S8–S9.
Elvin, P., Garner, A.P., 2005. Tumour invasion and metastasis: challenges facing drug discovery. Curr. Opin. Pharmacol. 5, 374–381.
Fallenstein, G.T., Hulce, V.D., Melvin, J.W., 1969. Dynamic mechanical properties of human brain tissue. J. Biomech. 2, 217–226.
Frieboes, H.B., Zheng, X., Sun, C.-H., Tromberg, B., Gatenby, R., Cristini, V., 2006. An integrated computational/experimental model of tumor invasion. Cancer Res. 66, 1597–1604.
Friedl, P., 2004. Prespecification and plasticity: shifting mechanisms of cell migration. Curr. Opin. Cell Biol. 16, 14–23.
Friedl, P., Wolf, A., 2003. Tumor cell invasion and migration: diversity and escape mechanisms. Nat. Rev., Cancer 3, 362–374.
Friedl, P., Hegerfeldt, Y., Tilisch, M., 2004. Collective cell migration in morphogenesis and cancer. Int. J. Dev. Biol. 48, 441–449 (Sp. Iss. SI).
Friedman, A., 2004. A hierarchy of cancer models and their mathematical challenges. Discrete Contin. Dyn. Syst., Ser. B 4, 147–159.
Garcke, H., Nestler, B., Stinner, B., 2004. A diffuse interface model for alloys with multiple components and phases, SIAM. J. Appl. Math. 64, 775–799.
Gatenby, R.A., Gawlinski, E.T., Gmitro, A.F., Kaylor, B., Gillies, R.J., 2006. Acid-mediated tumor invasion: a multidisciplinary study. Cancer Res. 66, 5216–5223.
Giese, A., Loo, M.A., Tran, N., Haskett, D., Coons, S.W., Berens, M.E., 1996. Dichotomy of astrocytoma migration and proliferation. Int. J. Cancer 67, 275–283.
Greenspan, H.P., 1976. On the growth and stability of cell cultures and solid tumors. J. Theor. Biol. 56, 229–242.
Hayot, C., Debeir, O., Van Ham, P., Van Damme, M., Kiss, R., Decaestecker, C., 2006. Characterization of the activities of actin-affecting drugs on tumor cell migration. Toxicol. Appl. Pharmacol. 211, 30–40.
Helmlinger, G., Yuan, F., Dellian, M., Jain, R.K., 1997. Interstitial pH and pO_2 gradients in solid tumors in vivo: high-resolution measurements reveal a lack of correlation. Nat. Med. 3, 177–182.
Holash, J., Maisonpierre, P.C., Compton, D., Boland, P., Alexander, C.R., Zagzag, D., Yancopoulos, G.D., Wiegand, S.J., 1999a. Vessel cooption, regression, and growth in tumors mediated by angiopoietins and VEGF. Science 284, 1994–1998.
Holash, J., Wiegand, S.J., Yancopoulos, G.D., 1999b. New model of tumor angiogenesis: dynamic balance between vessel regression and growth mediated by angiopoietins and VEGF. Oncogene 18, 5356–5362.
Huang, Q., Shen, H.M., Ong, C.N., 2005. Emodin inhibits tumor cell migration through suppression of the phosphatidylinositol 3-kinase-Cdc42/Rac1 pathway. Cell. Mol. Life Sci. 62, 1167–1175.
Jacqmin, D., 1999. Calculation of two-phase Navier–Stokes flows using phase-field modeling. J. Comp. Phys. 155, 96–127.
Jain, R.K., 2001. Delivery of molecular medicine to solid tumors: lessons from in-vivo imaging of gene expression and function. J. Control. Release 74, 7–25.
Jain, R.K., 2003. Molecular regulation of vessel maturation. Nat. Med. 9, 685–693.
Keller, P.J., Pampaloni, F., Stelzer, E.H.K., 2006. Life sciences require the third dimension. Curr. Opin. Cell Biol. 18, 117–124.
Khoshyomn, S., Lew, S., DeMattia, J., Singer, E.B., Penar, P.L., 1999. Brain tumor invasion rate measured in vitro does not correlate with Ki-67 expression. J. Neuro-Oncol. 45, 111–116.
Kim, J.S., Lowengrub, J.S., 2005. Phase field modeling and simulation of three-phase flows. Int. Free Bound. 7, 435.
Kim, J.S., Kang, K., Lowengrub, J.S., 2004a. Conservative multigrid methods for Cahn–Hilliard fluids. J. Comp. Phys. 193, 511–543.
Kim, J.S., Kang, K., Lowengrub, J.S., 2004b. Conservative multigrid methods for ternary Cahn–Hilliard systems. Comm. Math. Sci. 12, 53–77.
Kopfstein, L., Christofori, G., 2006. Metastasis: cell-autonomous mechanisms versus contributions by the tumor microenvironment. Cell. Mol. Life Sci. 63, 449–468.
Kuiper, R.A.J., Schellens, J.H.M., Blijham, G.H., Beijnen, J.H., Voest, E.E., 1998. Clinical research on antiangiogenic therapy. Pharmacol. Res. 37, 1–16.
Kumar, M., Krishnan, G., Arumainanthan, U., Singh, K., 2003. Endoscopic excision of a nasal glioma. Internet J. Otorhinolaryngol. 2 (1).

Kunkel, P., Ulbricht, U., Bohlen, P., Brockmann, M.A., Fillbrandt, R., Stavrou, D., Westphal, M., Lamszus, K., 2001. Inhibition of glioma angiogenesis and growth in vivo by systemic treatment with a monoclonal antibody against vascular endothelial growth factor receptor-2. Cancer Res. 61, 6624–6628.

Lah, T.T., Alonso, M.B.D., Van Noorden, C.J.F., 2006. Antiprotease therapy in cancer: hot or not? Exp. Op. Biol. Ther. 6, 257–279.

Lamszus, K., Kunkel, P., Westphal, M., 2003. Invasion as limitation to anti-angiogenic glioma therapy. Acta Neurochir., Suppl. 88, 169–177.

Lee, H., Lowengrub, J.S., Goodman, J., 2002. Modeling pinchoff and reconnection in a Hele–Shaw cell. I. The models and their calibration. Phys. Fluids 14, 492–513.

Leo, P.H., Lowengrub, J.S., Jou, H.-J., 1998. A diffuse interface model for elastically stressed solids. Acta Metall. 46, 2113–2130.

Less, J.R., Skalak, T.C., Sevick, E.M., Jain, R.K., 1991. Microvascular architecture in a mammary carcinoma: branching patterns and vessel dimensions. Cancer Res. 51, 265–273.

Li, C.H., Shan, S., Huang, Q., Braun, R.D., Lanzen, J., Hu, K., Lin, P., Dewhirst, M.W., 2000. Initial stages of tumor cell-induced angiogenesis: evaluation via skin window chambers in rodent models. J. Natl. Cancer Inst. 92, 143–147.

Li, X., Cristini, V., Nie, Q., Lowengrub, J., 2007. Nonlinear three-dimensional simulation of solid tumor growth. Discrete Contin. Dyn. Syst., Ser. B. 7, 581–604.

Lockett, J., Yin, S.P., Li, X.H., Meng, Y.H., Sheng, S.J., 2006. Tumor suppressive maspin and epithelial homeostasis. J. Cell Chem. 97, 651–660.

Lowengrub, J.S., Truskinovsky, L., 1998. Quasi-incompressible Cahn–Hilliard fluids and topological transitions. Proc. R. Soc. Lond., A 454, 2617–2654.

Macklin, P., Lowengrub, J.S., 2005. Evolving interfaces via gradients of geometry-dependent interior Poisson problems: application to tumor growth. J. Comp. Phys. 203, 191–220.

Macklin, P., Lowengrub, J.S., 2007. Nonlinear simulation of the effect of microenvironment on tumor growth. J. Theor. Biol. 245, 677–704.

McDougall, S.R., Anderson, A.R.A., Chaplain, M.A.J., 2006. Mathematical modeling of dynamic adaptive tumour-induced angiogenesis: clinical applications and therapeutic targeting strategies. J. Theor. Biol. 241, 564–589.

McLean, G.W., Carragher, N.O., Avizienyte, E., Evans, J., Brunton, V.G., Frame, M.C., 2005. The role of focal-adhesion kinase in cancer. A new therapeutic opportunity. Nat. Rev., Cancer 5, 505–515.

Naganuma, H., Kimurat, R., Sasaki, A., Fukamachi, A., Nukui, H., Tasaka, K., 1989. Complete remission of recurrent glioblastoma multiforme following local infusions of lymphokine activated killer cells. Acta Neurochir. 99, 157–160.

O'Connor, J.P.B., Jackson, A., Parker, G.J.M., Jayson, G.C., 2007. DCE-MRI biomarkers in the clinical evaluation of antiangiogenic and vascular disrupting agents. Br. J. Cancer 96, 189–195.

Ommaya, A.K., 1968. Mechanical properties of tissues of the nervous system. J. Biomech. 1, 127–138.

Padera, T.P., Stoll, B.R., Tooredman, J.B., Capen, D., di Tomaso, E., Jain, R., 2004. Cancer cells compress intratumour vessels. Nature 427, 695.

Page, D.L., Anderson, T.J., Sakamoto, G., 1987. Diagnostic Histopathology of the Breast Churchill. Livingstone, New York, pp. 219–222.

Patan, S., Munn, L.L., Tanda, S., Roberge, S., Jain, R.K., Jones, R.C., 2001a. Vascular morphogenesis and remodeling in a model of tissue repair: blood vessel formation and growth in the ovarian pedicle after ovariectomy. Circ. Res. 89, 723–731.

Patan, S., Tanda, S., Roberge, S., Jones, R.C., Jain, R.K., Munn, L.L., 2001b. Vascular morphogenesis and remodeling in a human tumor xenograft: blood vessel formation and growth after ovariectomy and tumor implantation. Circ. Res. 89, 732–739.

Pennacchietti, S., Michieli, P., Galluzzo, M., Mazzone, M., Giordano, S., Comoglio, P.M., 2003. Hypoxia promotes invasive growth by transcriptional activation of the met protooncogene. Cancer Cell 3, 347–361.

Plank, M.J., Sleeman, B.D., 2003. A reinforced random walk model of tumour angiogenesis and anti-angiogenic strategies. Math. Med. 20135–20181.

Plank, M.J., Sleeman, B.D., 2004. Lattice and non-lattice models of tumour angiogenesis. Bull. Math. Biol. 66, 1785–1819.

Preusser, M., Heinzl, H., Gelpi, E., Schonegger, K., Haberler, C., Birner, P., Marosi, C., Hegi, M., Gorlia, T., Hainfellner, J.A., 2006. Histopathologic assessment of hot-spot microvessel density and vascular patterns in glioblastoma: poor observer agreement limits clinical utility as prognostic factors: a translational research project of the European Organization for Research and Treatment of Cancer Brain Tumor Group. Cancer 107, 162–170.

Ridley, A.J., Schwartz, M.A., Burridge, K., Firtel, R.A., Ginsberg, M.H., Borisy, G., Parsons, J.T., Horwitz, A.R., 2003. Cell migration: integrating signals from front to back. Science 302, 1704–1709.

Rofstad, E., Halsor, E., 2002. Hypoxia-associated spontaneous pulmonary metastasis in human melanoma xenografts: involvement of microvascular hot spots induced in hypoxic foci by interleukin 8. Br. J. Cancer 86, 301–308.

Rubenstein, J.L., Kim, J., Ozawa, T., Zhang, M., Westphal, M., Deen, D.F., Shuman, M.A., 2000. Anti-VEGF antibody treatment of glioblastoma prolongs survival but results in increased vascular cooption. Neoplasia 2, 306–314.

Sahai, E., 2005. Mechanisms of cancer cell invasion. Curr. Opin. Genet. Dev. 15, 87–96.

Sanga, S., Sinek, J.P., Frieboes, H.B., Ferrari, M., Fruehauf, J.P., Cristini, V., 2006. Mathematical modeling of cancer progression and response to chemotherapy. Expert Rev. Anticancer Ther. 6, 1361–1376.

Seftor, E.A., Meltzer, P.S., Kirschmann, D.A., Pe'er, J., Maniotis, A.J., Trent, J.M., Folberg, R., Hendrix, M.J., 2002. Molecular determinants of human uveal melanoma invasion and metastasis. Clin. Exp. Metastasis 19, 233–246.

Shweiki, D., Itin, A., Soffer, D., Keshet, E., 1999. Vascular endothelial growth factor induced by hypoxia may mediate hypoxia-initiated angiogenesis. Nature 359, 843–845.

Sierra, A., 2005. Metastases and their microenvironments: linking pathogenesis and therapy. Drug Resist. Updat. 8, 247–257.

Sinek, J., Frieboes, H.B., Zheng, X., Cristini, V., 2004. Two-dimensional chemotherapy simulations demonstrate fundamental transport and tumor response limitations involving nanoparticles. Biomed. Microdev. 6 (4), 297–309.

Skinner, S.A., 1990. Microvascular architecture of experimental colon tumors in the rat. Cancer Res. 50, 2411–2417.

Steeg, P.S., 2003. Angiogenesis inhibitors: motivators of metastasis? Nat. Med. 9, 822–823.

Sun, S., Wheeler, M.F., Obeyesekere, M., Patrick Jr., C., 2005. Multiscale angiogenesis modeling using mixed finite element methods. Multiscale Model. Simul. 4, 1137–1167.

Takano, S., Yoshii, Y., Kondo, S., Suzuki, H., Maruno, T., Shirai, S., Nose, T., 1996. Concentration of vascular endothelial growth factor in the serum and tumor tissue of brain tumor patients. Cancer Res. 56, 2185–2190.

Toker, A., Yoeli-Lerner, M., 2006. Akt signaling and cancer: surviving but not moving on. Cancer Res. 66, 3963–3966.

Tysnes, B.B., Mahesparan, R., 2001. Biological mechanisms of glioma invasion and potential therapeutic targets. J. Neurooncol. 53, 129–147.

Vajkoczy, P., Farhadi, M., Gaumann, A., Heidenreich, R., Erber, R., Wunder, A., Tonn, J.C., Menger, M.D., Breier, G., 2002. Microtumor growth initiates angiogenic sprouting with simultaneous expression of VEGF, VEGF receptor-2, and angiopoietin-2. J. Clin. Invest. 109, 777–785.

van Kempen, L.C.L.T., Ruiter, D.J., van Muijen, G.N.P., Coussens, L.M., 2003. The tumor microenvironment: a critical determinant of neoplastic evolution. Eur. J. Cell Biol. 82, 539–548.

Wise, S.M., Lowengrub, J.S., Kim, J.S., Johnson, W.C., 2004. Efficient phase-field simulation of quantum dot formation in a strained hetero-epitaxial film. Superlattices Microstruct. 36, 293–304.

Wolf, K., Friedl, P., 2006. Molecular mechanisms of cancer cell invasion and plasticity. Br. J. Dermatol. 154, 11–15.

Wurzel, M., Schaller, C., Simon, M., Deutsch, A., 2005. Cancer cell invasion of brain tissue: guided by a prepattern? J. Theor. Med. 6, 21–31.

Yamaguchi, H., Wyckoff, J., Condeelis, J., 2005. Cell migration in tumors. Curr. Opin. Cell Biol. 17, 559–564.

Yin, S.P., Lockett, J., Meng, Y.H., Biliran, H., Blouse, G.E., Li, X.H., Reddy, N., Zhao, Z.M., Lin, X.L., Anagli, J., Cher, M.L., Sheng, S.J., 2006. Maspin retards cell detachment via a novel interaction with the urokinase-type plasminogen activator/urokinase-type plasminogen activator receptor system. Cancer Res. 66, 4173–4181.

Zagzag, D., Amirnovin, R.,Greco, M.A., Yee, H., Holash, J., Wiegand, S.J., Zabski, S., Yancopoulos, G.D., Grumet, M., 2000. Vascular apoptosis and involution in gliomas precede neovascularization: a novel concept for glioma growth and angiogenesis.

Zheng, X., Wise, S., Cristini, V., 2005. Nonlinear simulation of tumor necrosis, neo-vascularization and tissue invasion via an adaptive finite-element/level-set method. Bull. Math. Biol. 67, 211–259.